A&A 470, 97–104 (2007)
DOI: 10.1051/0004-6361:20077265

Astronomy & Astrophysics

VLBI observations of nineteen GHz-peaked-spectrum radio sources at 1.6 GHz

X. Liu[1], L. Cui[1,2], W.-F. Luo[1,2], W.-Z. Shi[1,2], and H.-G. Song[1]

[1] National Astronomical Observatories/Urumqi Observatory, CAS, 40-5 South Beijing Road, Urumqi 830011, PR China
e-mail: liux@ms.xjb.ac.cn
[2] Graduate University of the Chinese Academy of Sciences, Beijing 100049, PR China

Received 9 February 2007 / Accepted 12 April 2007

ABSTRACT

Aims and Methods. We present the results of VLBI observations of nineteen GHz-peaked-spectrum (GPS) radio sources at 1.6 GHz. Of them, 15 sources are selected from the Parkes half-jansky (PHJ) sample (Snellen et al. 2002, MNRAS, 337, 981), and 4 others are from our previous observation list. We aimed at imaging the structure of GPS sources, searching for compact symmetric objects (CSOs) and studying the absorption for the convex radio spectra of GPS sources.
Results. We obtained total-intensity 1.6 GHz VLBI images of 17 sources for the first time. Of them, 80% show a mini-double-lobe radio structure, indicating that they are CSOs or candidates, and their host AGNs could be edge-on to us. This result suggests that there is a high incidence of mini double-lobe sources (or CSOs) in the PHJ sample. The sources J0323+0534, J1135−0021, J1352+0232, J2058+0540, J2123−0112, and J2325−0344 are classified as CSOs with measured redshift, showing double-lobe structure with sizes of <1 kpc. Three sources J1057+0012, J1600−0037, and J1753+2750 are considered as core-jet sources according to their morphologies and flux variability.

Key words. galaxies: nuclei – quasars: general – radio continuum: galaxies – galaxies: active

1. Introduction

The GHz-peaked-spectrum (GPS) radio sources are powerful ($P_{1.4\,\mathrm{GHz}} \geq 10^{25}\,\mathrm{W\,Hz^{-1}}$) and compact ($\leq$1 kpc), they have convex radio spectra, and they make up a significant fraction ($\approx$10%) of the bright radio-source sample; see O'Dea (1998) for a review. In general, the presence of large-scale emission associated with GPS galaxies is rare, about a few percent in a GPS sample (Stanghellini et al. 2005). Most GPS sources appear to be truly compact and isolated.

Their small size is most likely due to their youth ($<10^4$ years) according to a spectral aging analysis (Murgia 2003). A couple of GPS sources are certainly young radio sources whose kinematic age from lobe proper motions has been measured and these sources are also identified as compact symmetric objects (CSOs). There is compelling evidence in favour of the youth scenario of GPS sources and CSOs, see e.g. Owsianik & Conway (1998), Tschager et al. (2000), Polatidis & Conway (2003), and Orienti et al. (2007). The GPS sources and CSOs are the key objects to study the early evolution of powerful radio-loud AGN. A unification scenario assumes that GPS sources evolve into compact steep spectrum sources (1–15 kpc), which in turn evolve into classical extended radio sources (>15 kpc), i.e. FR I/II radio sources (Fanti et al. 1995; Snellen et al. 2000; de Vries et al. 2007).

GPS *galaxies* are dominated by lobe/jet emission on both sides of the central engine and are thought to be relatively free of beaming effects. The GPS galaxies show very low polarization (about less than 0.5% at 5 GHz, Dallacasa 2004; Xiang et al. 2006). The low integrated polarization could be due to large Faraday depths around the radio source, which would depolarize the radio emission, implying that their host-AGNs are probably edge-on to us.

Since GPS sources live in the narrow-line region of AGN, it is likely that their low-frequency radio emission will be absorbed due to either synchrotron self-absorption or free-free absorption, giving rise to a peaked radio spectrum. Therefore, GPS sources are also suitable for studying radio absorption and scattering in AGNs.

We have carried out EVN (European VLBI Network) observations of 19 GPS sources, 15 of them from the Parkes half-jansky (PHJ) sample (Snellen et al. 2002) with declination >−5° and not observed with VLBI before. Four sources are from our previous observation list, which we observed with the EVN at 2.3/8.4 GHz and/or 5 GHz (see Xiang et al. 2005, 2006). We aimed at imaging the GPS sources at 1.6 GHz, in order to confirm whether the GPS sources are double-lobe sources and to find CSO candidates. For the sources with observations at 2.3, 5.0, and 8.4 GHz, the 1.6 GHz images will provide more information on their source structure and intensity at a lower frequency, for further spectral study of the GPS sources in the future.

2. Observations and data reduction

The observations were carried out on 3 March 2006 at 1.65 GHz using the MK5 recording system with a bandwidth of 32 MHz and sample rate of 256 Mbps in dual circular polarization. The EVN antennae in this experiment were Effelsberg, Westerbork, Jodrell, Medicina, Noto, Onsala, Torun, Hartebeesthoek, Urumqi, and Shanghai. Snapshot observations of 19 sources (Table 1) in a total of 24 h were made, and OQ208

Table 1. The GPS sources.

1 Source	2	3 id	4 m_R	5 z	6 pc/mas	7 θ mas	8 L pc	9 $S_{1.4}$ mJy	10 $S_{2.7}$ Jy	11 α_l	12 α_h	13 ν_m GHz	14 S_m Jy	15 ref.
J0210+0419	B0208+040	G	18.3 Ks	1.5*	6.1	90		948	0.56		0.80	0.4	1.3	1
J0323+0534	4C+05.14	G	19.2	0.1785	2.7	180	490	2793	1.60		0.85	0.4	7.1	1
J0433−0229	4C−02.17	G	19.1	0.530	5.1	80	408	1462	1.04		0.52	0.4	3.0	1
J0913+1454	B0910+151	G	22.9	0.47*	4.9	80		881	0.54		0.75	0.6	1.1	1
J1057+0012	B1054+004	G	22.3	0.65*	5.5	80?		898	0.58		0.67	0.4	1.6	1
J1109+1043	B1107+109	G	22.6	0.55*	5.2	60		1481	0.80		0.94	0.5	2.4	1
J1135−0021	4C−00.45	G	21.9	0.975	6.0	120	720	1268	0.76		0.78	0.4	2.9	1
J1203+0414	B1200+045	QSO	18.8	1.221	6.1	75	458	1146	0.85		0.45	0.4	1.4	1
J1352+0232	B1349+027	G	20.0	0.607	5.4	170	918	1145	0.78		0.58	0.4	2.0	1
J1352+1107	4C+11.46	G	21.0	0.891	5.9	50	295	1538	0.78		1.03	0.4	3.6	1
J1600−0037	B1557−004	G				50		1168	0.54		1.17	1.0	1.2	1
J1648+0242	4C+02.43	G	22.1	0.824	5.8				0.61			0.4	3.4	1
J2058+0540	4C+05.78	G	23.4	1.381	6.1	160	970	1213	0.65		0.95	0.4	3.1	1
J2123−0112	B2121−014	G	23.3	1.158	6.1	80	488	1087	0.64	–0.56	0.75	0.5	1.8	2
J2325−0344	B2322−040	G	23.5	1.509	6.0	75	450	1224	0.91	–0.42	0.75	1.4	1.3	2
J0917+1113	B0914+114	EF				190		800	0.31	–0.1	1.6	0.3	2.3	3
J1753+2750	B1751+278	G	21.7	0.86*	5.9	50		625	0.46	–0.27	0.57	1.4	0.6	2
J1826+2708	B1824+271	G	22.9			45		332	0.23	–0.39	0.75	1.0	0.4	2
J2325+7917	B2323+790	G	19.5V			32		1136		–0.3	0.75	1.4	1.2	2

and DA193 were observed as calibrators. The data correlation was completed at JIVE.

The total flux densities of the sources were also measured at 5 GHz with Urumqi 25 m telescope in order to find any flux variability, the values are listed in Table 2. Columns 2–4 are flux densities at 5.0 GHz (PKS90), 4.85 GHz (Gregory & Condon 1991; and Griffith et al. 1995), and 4.85 GHz flux measured with the Urumqi 25 m telescope on 2007/1/24 (J1648+0242, J2058+0540, 1824+271, and 2121−014 were not well measured due to source confusion or weak); Col. 5 is a flux variability computed from Cols. 3 and 4.

The Astronomical Image Processing System (AIPS) was used for editing, a priori calibration, fringe-fitting, self-calibration, imaging, and model-fitting of the data.

Table 2. Source total flux density at 5 GHz and possible variability.

Source	$S_{5.0}$ mJy	$S_{4.85}$ mJy	$S_{4.85Ur}$ mJy	$\delta S_{4.85}$ %
J0210+0419	300	298 ± 19	302 ± 10	1.3 ± 3.1
J0323+0534	830	819 ± 44	868 ± 9	6.0 ± 4.6
J0433−0229	640	640 ± 35	637 ± 14	−0.5 ± 3.3
J0913+1454	300	315 ± 43	297 ± 8	−5.7 ± 10.3
J1057+0012	370	396 ± 23	351 ± 6	−11.4 ± 3.6
J1109+1043	400	408 ± 56	428 ± 8	4.9 ± 12.4
J1135−0021	440	446 ± 25	427 ± 8	−4.3 ± 3.6
J1203+0414	520	640 ± 35	611 ± 7	−4.5 ± 4.1
J1352+0232	470		469 ± 7	
J1352+1107	410	447 ± 62	418 ± 5	−6.5 ± 11.9
J1600−0037	180	187 ± 14	212 ± 3	13.4 ± 6.9
J1648+0242	260	337 ± 20		
J2058+0540	340	356 ± 21		
B2121−014	320	345 ± 21		
B2322−040	500	524 ± 29	545 ± 20	4.0 ± 1.9
B0914+114	140	134 ± 19	140 ± 1	4.5 ± 14.1
B1751+278		298 ± 39	292 ± 6	−2.0 ± 10.8
B1824+271		122 ± 17		
B2323+790			491 ± 7	
OQ208		2421 ± 217	2514 ± 12	3.8 ± 8.8

3. Results and comments on individual sources

We list the basic information of the sources in Table 1: Cols. (1), (2) source names; (3) optical identification (G: galaxy, QSO: quasar, EF: empty field); (4) optical magnitude; (5) redshift (de Vries et al. 2007, those with * are a photometric estimated by Tinti et al. 2005); (6) linear scale factor pc/mas (H_0 = 71 km s^{-1} Mpc^{-1} and q_0 = 0.5 have been assumed); (7) maximum angular size from the observation; (8) maximum linear size; (9) 1.4 GHz flux density from the NVSS; (10) 2.7 GHz flux density from Snellen sample and the NED; (11) low frequency spectral index; (12) higher frequency spectral index (computed from Cols. 9 and 10), $S \propto \nu^{-\alpha}$; (13) turnover frequency; (14) peak flux density; (15) references for the spectral information, 1 Snellen et al. (2002), 2 de Vries et al. (1997), 3 Stanghellini et al. (1998). The parameters derived from the VLBI images are in Table 3: columns give (1) source name and possible classification (CSOc: CSO candidate, cj: core-jet); (2) total cleaned flux density of image at 1.6 GHz; (3) component identification labled to Xiang et al. 2002, 2005, 2006; (4), (5) peak and integral intensity of a fitted Gaussian component at 1.6 GHz in the AIPS task JMFIT; (6), (7) major/minor axes and position angle of component at 1.6 GHz; (8), (9) distance and position angle relative to the first component; (10) brightness temperature of component. We comment here on the results of each source and give a short discussion. We use $S \propto \nu^{-\alpha}$ to define the spectral index. Optical information and redshifts of the GPS sources in the PHJ sample are given by de Vries et al. (2007), as listed in Table 1.

3.1. J0210+0419 (PKS B0208+040)

The 1.6 GHz VLBI image (Fig. 1) is the first VLBI image of the source. It shows a double-lobe structure and is most likely a CSO. Optical observations did not result in an identification with

Table 3. The component parameters of the VLBI images at 1.6 GHz.

1 Name class	2 $S_{\rm vlbi}$ mJy	3 Comp	4 Sp mJy	5 Sint mJy	6 $\theta_1 \times \theta_2$ mas × mas	7 PA °	8 d mas	9 PA °	10 $T_{\rm b}$ 10^8 K°
J0210+0419	715	A	290	375	5.7 × 2.9	169	0		11.9
CSOc		B	118	205	10 × 3.6	175	68.2 ± 0.1	–153.2 ± 0.1	2.2
J0323+0534	1497	A	536	1270	32.6 × 11.1	70	0		0.5
CSO		B	117	548	57.5 × 21.7	18	122.7 ± 2.9	–167.2 ± 0.4	0.1
J0433−0229	1095	A	407	1045	14.5 × 4.7	171	0		2.4
CSOc/cj		B	49	111	9.9 × 5.5	88	53.0 ± 0.3	164.4 ± 0.2	0.3
J0913+1454	796	A	211	501	8.2 × 4.9	65	0		2.1
CSOc		B	55	157	8.9 × 6.2	80	56.8 ± 0.1	73.3 ± 0.1	0.4
J1057+0012	810	A	381	550	3.6 × 2.7	6.6	0		17.5
cj		B	37	58	6.2 × 2.1	9.7	9.7 ± 0.2	114.8 ± 0.9	1.3
J1109+1043	1370	A	420	984	5.7 × 4.7	110	0		6.6
CSOc		B	143	311	5.4 × 4.2	91	46.3 ± 0.1	104.4 ± 0.1	2.6
J1135−0021	1025	A	279	454	6.6 × 2.7	142	0		4.9
CSO		B	143	271	8.6 × 3.0	153	85.8 ± 0.1	164.4 ± 0.1	1.7
J1203+0414	1029	A	571	850	4.7 × 2.9	107	0		25.1
CSOc		B	51	81	5.0 × 3.8	78	18.1 ± 0.2	103.0 ± 0.4	1.6
		C	31	35	6 × 6	0	58.2 ± 0.2	104.2 ± 0.2	1.9
J1352+0232	885	A	173	480	7.4 × 4.5	53	0		2.1
CSO		B	30	120	8.9 × 6.3	110	165.7 ± 0.3	–111.9 ± 0.1	0.2
J1352+1107	896	A	198	395	8.1 × 5.4	11.7	0		2.0
CSOc/cj		B	106	202	6.8 × 6.3	10	3.5 ± 0.1	53.1 ± 0.1	1.1
J1600−0037	936	A	394	607	5.4 × 4.1	157	0		
cj		B	125	255	7.9 × 5.0	86	24.7 ± 0.1	83.5 ± 0.1	
J2058+0540	914	A	356	513	7.6 × 3.7	163	0		8.2
CSO		B	182	403	12.6 × 4.5	128	127.2 ± 0.1	172.1 ± 0.1	2.3
B2121−014	976	A	363	594	5.1 × 3.9	123	0		10.4
CSO		C	191	415	7.4 × 5.0	126	59.4 ± 0.1	85.4 ± 0.1	2.9
B2322−040	965	A	229	509	14.6 × 3.3	161	0		3.6
CSO		B	74	160	11.7 × 5.3	162	40.6 ± 0.2	171.3 ± 0.1	0.8
		C	65	196	19.3 × 4.7	1	22.0 ± 0.4	171.1 ± 0.2	0.5
B0914+114	578	A	37	50	4.9 × 2.7	16	0		
CSO		B	29	65	9.1 × 4.3	66	45.6 ± 0.1	80.1 ± 0.1	
		C	242	360	4.2 × 3.9	90	84.2 ± 0.1	81.6 ± 0.1	
		E	28	40	4.4 × 3.4	63	86.1 ± 0.1	–95.9 ± 0.1	
B1751+278	596	A	400	522	4.8 × 2.9	71	0		14.5
cj		B	26	37	8 × 3	15	20.5 ± 0.1	–128.6 ± 0.2	0.5
		C	12.4	21	7 × 5	59	26.6 ± 0.3	–119.8 ± 0.3	0.2
		D	8	20	19.5 × 3.6	176	41.4 ± 0.4	–104.4 ± 0.8	0.1
B1824+271	296	A	145	174	3.9 × 2.1	164	0		
CSO		B	42	69	6.1 × 4.3	137	21.8 ± 0.1	–83.4 ± 0.1	
B2323+790	900	A	439	621	5.8 × 2.1	159	0		
CSOc		B+C	107	155	7.9 × 3.1	118	19.2 ± 0.1	–71.1 ± 0.1	

a lower limit of $m_R > 24.1$, but it is identified with a magnitude of $Ks = 18.3$ (de Vries et al. 2007).

3.2. J0323+0534 (4C+05.14)

The 1.6 GHz VLBI image (Fig. 2) is the first VLBI image of the source, and it exhibits a strong diffuse component and a weak extended component in the south. Both are probably lobe emission. About 38% total flux density (estimated from Table 1) is resolved out in the VLBI image, due to the diffuse components. For its size of 490 pc, the source can be a CSO.

3.3. J0433−0229 (4C−02.17)

The 1.6 GHz VLBI image (Fig. 3) is the first VLBI image of the source, and the main component is diffuse and extended in the north-south direction and a possible weak component in the south. About 18% total flux density (estimated from Table 1) is resolved out in the VLBI image. Either a core-jet or a CSO classification is possible for the source.

3.4. J0913+1454 (PKS B0910+151)

The 1.6 GHz VLBI image (Fig. 4) is the first VLBI image of the source. It shows a double structure, and both components are further resolved. There is probably a hotspot imbedded in the bright one. We consider it a CSO candidate.

3.5. J1057+0012 (PKS B1054+004)

The 1.6 GHz VLBI image (Fig. 5) is the first VLBI image of the source. There is a bright compact component followed by a secondary component and a series of possibly weak components in the east, indicating this is a core-jet source. A flux variability

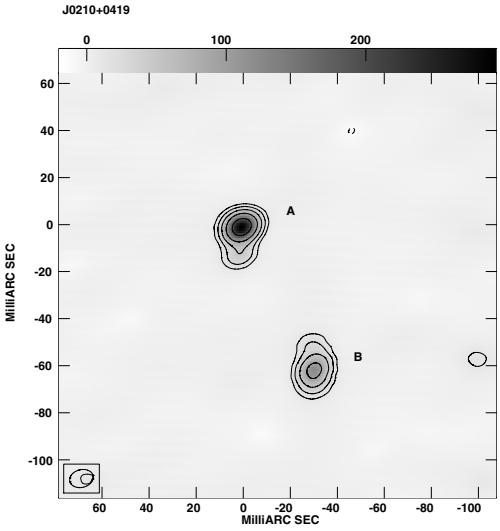

Fig. 1. J0210+0419 at 1.65 GHz. The restoring beam is 10.2 × 7.5 mas with PA −75.5°, the peak is 293 mJy/beam, the contours are 12 mJy/beam times levels –1, 1, 2, 4, 8, 16, 32, 64, 100, 200, 400, 800, and the same levels are used in the following images. The grey scale unit is mJy.

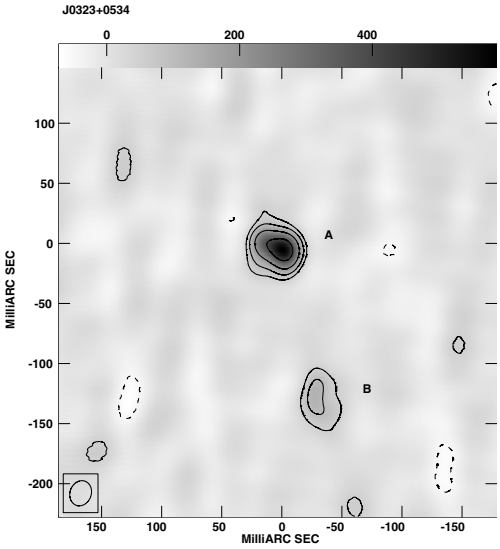

Fig. 2. J0323+0534 at 1.65 GHz. The restoring beam is 21.3 × 17.7 mas with PA −20.2°, the peak is 586 mJy/beam, and the first contour is 50 mJy/beam.

of (−11.4 ± 3.6)% over 15 years at 5 GHz, as reported in Table 2, is consistent with the core-jet classification.

3.6. J1109+1043 (PKS B1107+109)

The 1.6 GHz VLBI image (Fig. 6) is the first VLBI image of the source. It is a double structure and can be a CSO candidate. The total flux density (1270 mJy estimated from Table 1) is completely restored in the VLBI image (1370 mJy, increased by 8%). There is also an indication of total flux increasing (4.9 ± 12.4)% at 5 GHz in Table 2 but with a large error.

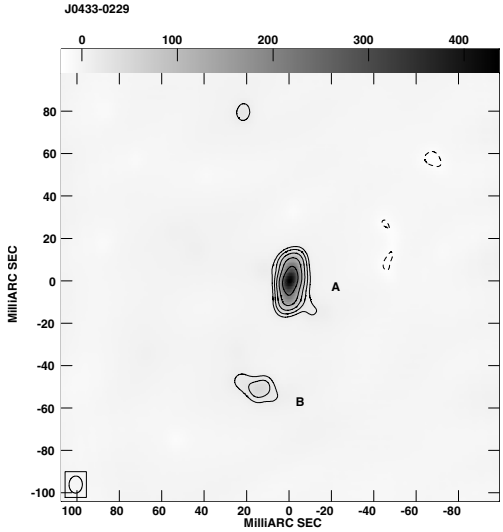

Fig. 3. J0433−0229 at 1.65 GHz. The restoring beam is 8.0 × 6.3 mas with PA −1.7°, the peak is 435 mJy/beam, and the first contour is 15 mJy/beam.

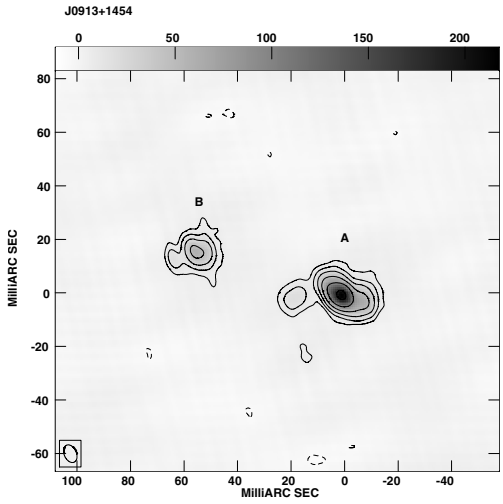

Fig. 4. J0913+1454 at 1.65 GHz. The restoring beam is 6.9 × 4.6 mas with PA 24.4°, the peak is 217 mJy/beam, and the first contour is 6 mJy/beam.

3.7. J1135−0021 (4C−00.45)

The 1.6 GHz VLBI image (Fig. 7) is the first VLBI image of the source. It shows a double-lobe structure, and with its size of 720 pc, we classify the source as a CSO.

3.8. J1203+0414 (PKS B1200+045)

The 1.6 GHz VLBI image (Fig. 8) is the first VLBI image of the source. The triple structure may consist of a core and two-sided emission, or a one-sided core-jet source. The quasar, as newly identified by de Vries et al. (2007), is possibly a core-jet one, but still we keep the source as a CSO candidate.

3.9. J1352+0232 (PKS B1349+027)

The 1.6 GHz VLBI image (Fig. 9) is the first VLBI image of the source. It shows a double-lobe like structure, and we consider it as a CSO because of its size of 918 pc.

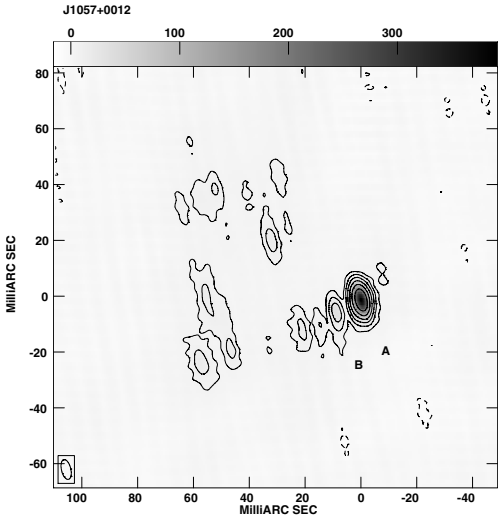

Fig. 5. J1057+0012 at 1.65 GHz. The restoring beam is 7.3 × 3.3 mas with PA 13.4°, the peak is 390 mJy/beam, and the first contour is 6 mJy/beam.

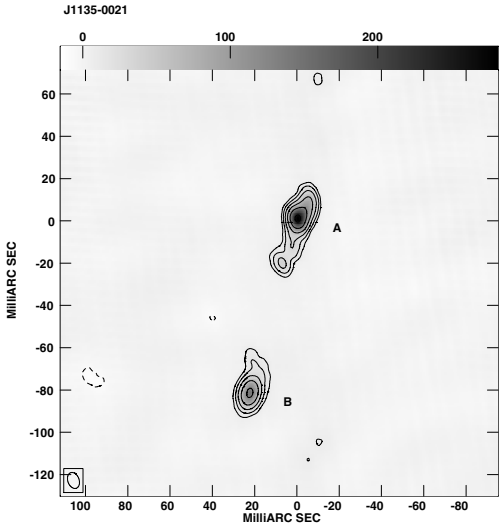

Fig. 7. J1135−0021 at 1.65 GHz. The restoring beam is 7.8 × 5.3 mas with PA 20.4°, the peak is 281 mJy/beam, and the first contour is 8 mJy/beam.

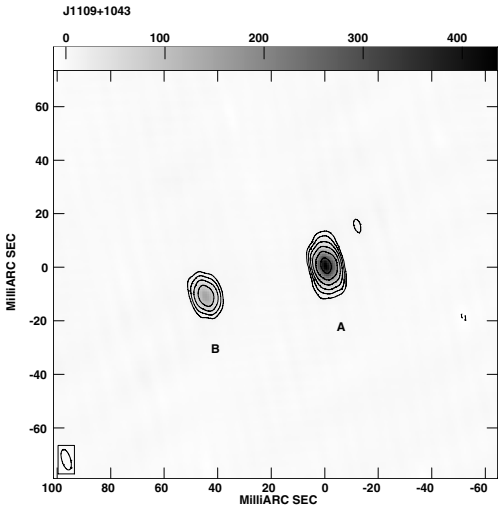

Fig. 6. J1109+1043 at 1.65 GHz. The restoring beam is 7.9 × 3.3 mas with PA 16.5°, the peak is 434 mJy/beam, and the first contour is 10 mJy/beam.

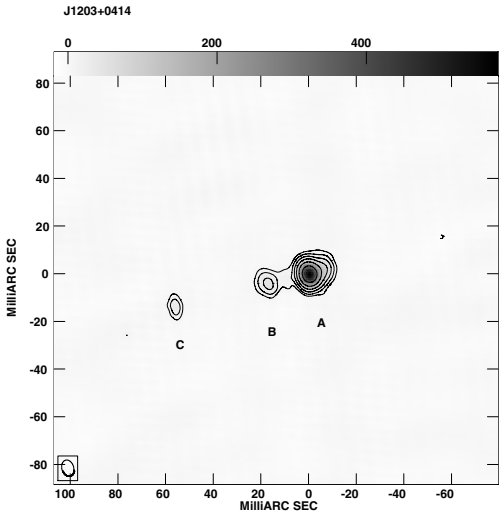

Fig. 8. J1203+0414 at 1.65 GHz. The restoring beam is 7.0 × 4.9 mas with PA 15.2°, the peak is 575 mJy/beam, and the first contour is 10 mJy/beam.

3.10. J1352+1107 (4C+11.46)

The 1.6 GHz VLBI image (Fig. 10) is the first VLBI image of the source. It appears to have a compact double structure or a core-jet, and seems diffuse emission around the source. About 30% total flux density (estimated from Table 1) is resolved out in the VLBI image. Either a corejet or a compact double classification is possible.

3.11. J1600−0037 (PKS B1557−004)

The 1.6 GHz VLBI image (Fig. 11) is the first VLBI image of the source, and it has an overall double structure, while the eastern component has some extension in the west-east direction. A flux variability of (13 ± 6.9)% at 5 GHz in Table 2 may suggest this is a core-jet source.

3.12. J1648+0242 (4C+02.43)

The GPS source is not detected with VLBI. It is an NVSS double-lobe source, and totally resolved out in the VLBI observation.

3.13. J2058+0540 (4C+05.78)

The 1.6 GHz VLBI image (Fig. 12) is the first VLBI image of the source. It shows a double-lobe source, and because of its size of 970 pc, we suggest this is a CSO.

3.14. PKS B2121−014

The 1.6 GHz VLBI image (Fig. 13) shows a double-lobe structure, and it is similar to that at 2.3 and 5 GHz (Xiang et al. 2005, 2006), except that a weak jet-like emission "B" appearing at 2.3 and 5 GHz is missing, probably due to absorption at the lower

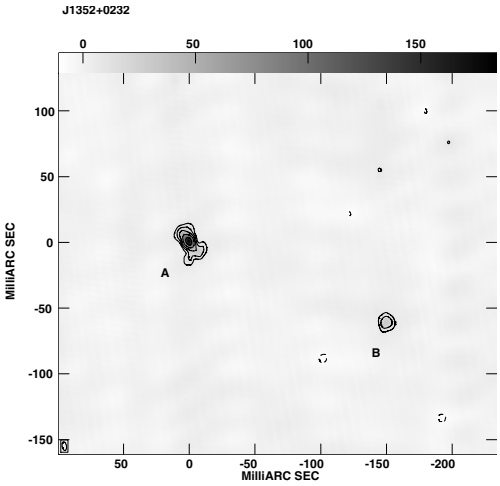

Fig. 9. J1352+0232 at 1.65 GHz. The restoring beam is 6.7 × 3.2 mas with PA 9.9°, the peak is 183 mJy/beam, and the first contour is 8 mJy/beam.

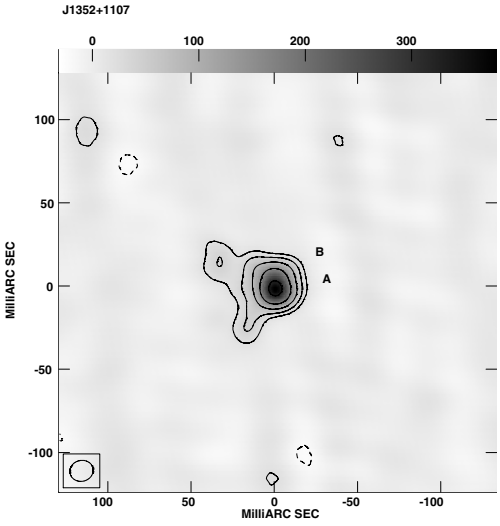

Fig. 10. J1352+1107 at 1.65 GHz. The restoring beam is 14.0×12.5 mas with PA −75.3°, the peak is 379 mJy/beam, and the first contour is 20 mJy/beam.

frequency 1.6 GHz. The source is a CSO for the source size of 488 pc.

3.15. PKS B2322−040

The 1.6 GHz VLBI image (Fig. 14) exposes a central emission region between the two lobes "A" and "B", which is probably a core embedded in the central region. The "core" emission is not detected at higher frequencies (Xiang et al. 2005, 2006), but it emerges at 1.6 GHz near the peak frequency (1.4 GHz) of the GPS source. There is a flux increase of (4.0±1.9)% over 15 years at 5 GHz (Table 2), suggesting that the core is currently active. The source can be a CSO from its size of 450 pc.

3.16. PKS B0914+114

The 1.6 GHz VLBI image (Fig. 15) exhibits a core "A", jet feature "B", and two lobes "C" and "E". The western one "E" emerges at this frequency. Labiano et al. (2007) have identified

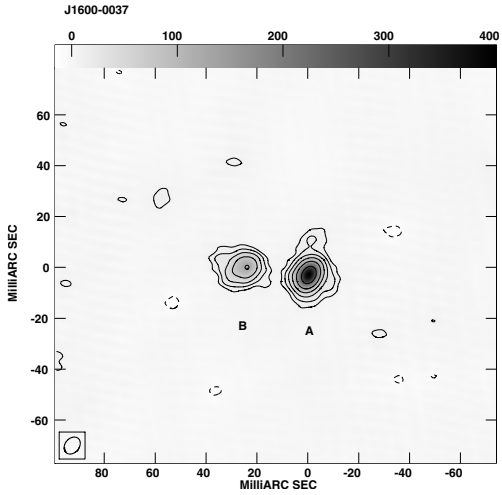

Fig. 11. J1600−0037 at 1.65 GHz. The restoring beam is 7.4 × 5.5 mas with PA −39.8°, the peak is 400 mJy/beam, and the first contour is 8 mJy/beam.

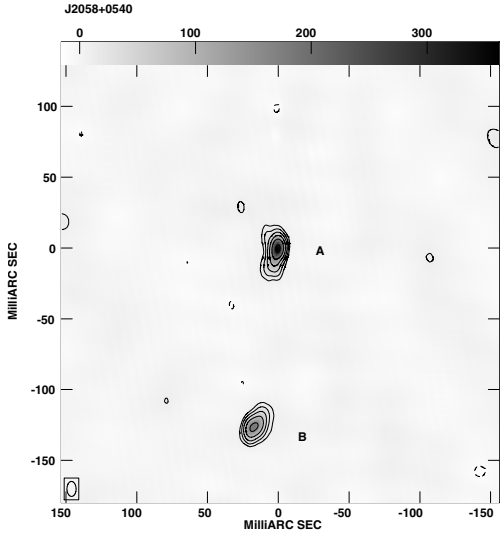

Fig. 12. J2058+0540 at 1.65 GHz. The restoring beam is 10.6 × 6.5 mas with PA 0.7°, the peak is 362 mJy/beam, and the first contour is 10 mJy/beam.

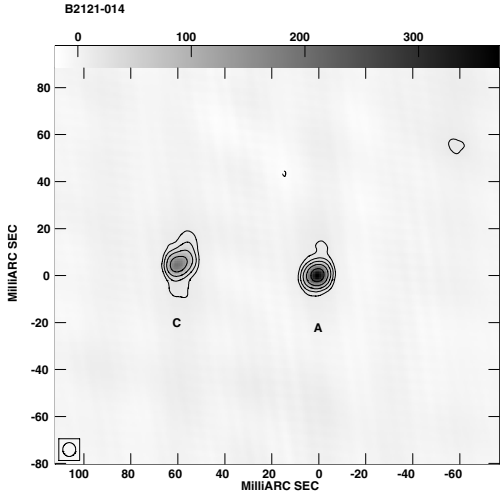

Fig. 13. 2121−014 at 1.65 GHz. The restoring beam is 5.9 × 5.5 mas with PA −1.4°, the peak is 370 mJy/beam, and the first contour is 15 mJy/beam.

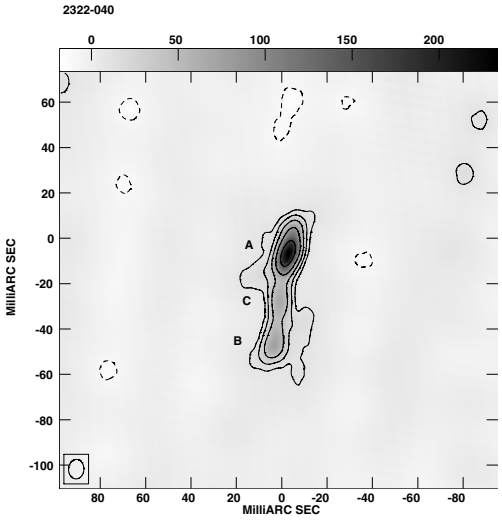

Fig. 14. 2322−040 at 1.65 GHz. The restoring beam is 8.6 × 6.8 mas with PA −2.1°, the peak is 233 mJy/beam, and the first contour is 10 mJy/beam.

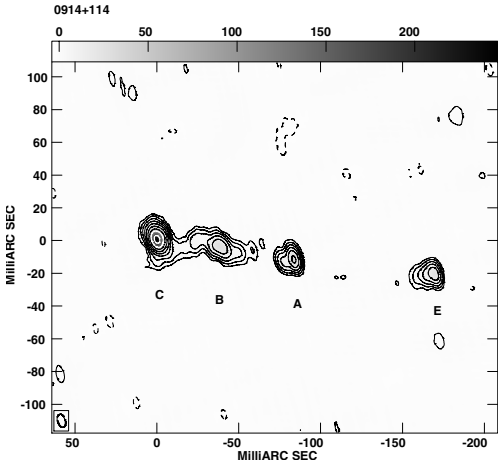

Fig. 15. 0914+114 at 1.65 GHz. The restoring beam is 8.3 × 4.7 mas with PA 16.8°, the peak is 246 mJy/beam, and the first contour is 1 mJy/beam.

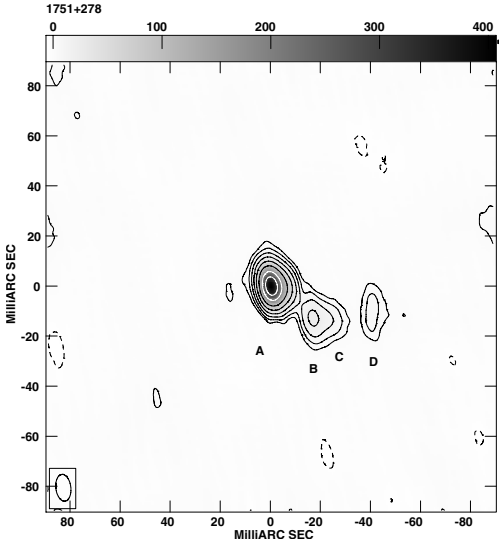

Fig. 16. 1751+278 at 1.65 GHz. The restoring beam is 10.7 × 6.0 mas with PA 7.0°, the peak is 406 mJy/beam, and the first contour is 3 mJy/beam.

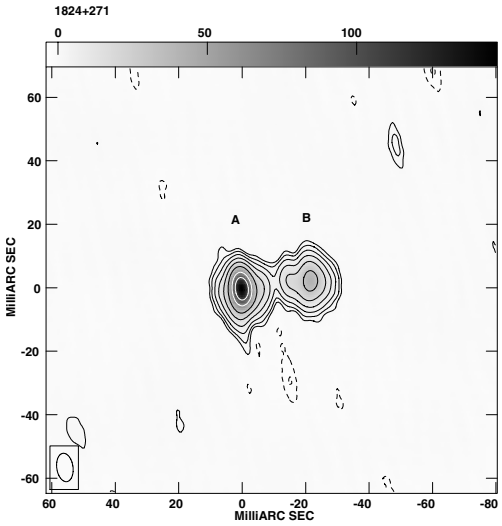

Fig. 17. 1824+271 at 1.65 GHz. The restoring beam is 9.0×5.1 mas with PA 8.1°, the peak is 146 mJy/beam, and the first contour is 1 mJy/beam.

an empty field (>25 m_R) at the FIRST position of the source and conclude that the previously identified, nearby disk galaxy (a redshift of 0.178) is not the host to this radio source 0914+114. For the typical compact, symmetric structure, we consider the source is a CSO.

3.17. 1751+278 (MG2 J175301+2750)

The 1.6 GHz structure (Fig. 16) is similar to what we got before at 1.6 GHz (Xiang et al. 2002), which confirms that there is jet-like emission "C" and "D" associated with the southern component "B", indicating this is a core-jet source.

3.18. B2 1824+271

The 1.6 GHz VLBI image (Fig. 17) exposes a symmetric double structure and jet-like emission associated with the two lobes, confirming this is a CSO as we suggested (Xiang et al. 2006).

3.19. [WB92] 2323+790

The 1.6 GHz image (Fig. 18) shows a central component "A" and a weak one "B+C" in the northwest, and the components "A" and "B+C" show steep spectra between 1.6 GHz and 5 GHz (Xiang et al. 2006). The source can be a CSO candidate.

4. Discussion

In the sample (Table 1), J1648+0242 is an NVSS double source and is not detected in this VLBI observation; all others are point-like in the NVSS images, indicating that GPS sources are compact. Except for four sources (J1057+0012, J1352+1107, J1600−0037, and 1751+278), 14 out of 18 sources exhibit a double or triple VLBI structure and can be CSOs or CSO candidates, though some of them have no measured redshift. The sources with redshift show double or triple structure with sizes <1 kpc, suggesting these GPS sources are certainly compact and likely CSOs.

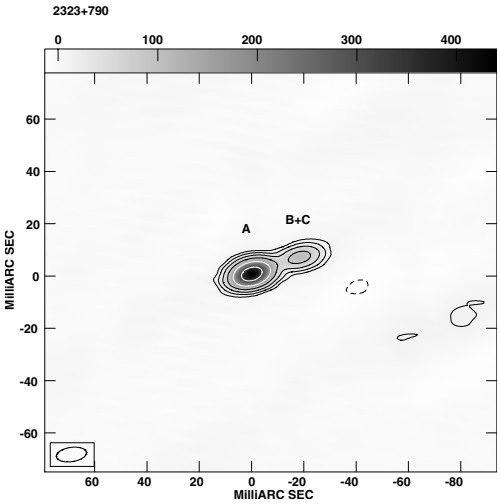

Fig. 18. 2323+790 at 1.65 GHz. The restoring beam is 11.6 × 5.4 mas with PA −82°, the peak is 438 mJy/beam, and the first contour is 10 mJy/beam.

The mini double-lobe sources or CSOs could be more stable in flux density than other types of compact sources. We measured the flux densities for the sources (Table 2) at 4.85 GHz and compared them with the values observed 15 years ago. We find that 12 among the 14 GPS sources are probably stable in flux (1σ level), and two sources (J1057+0012 and J1600−0037) show about 10% variability on the 3σ and 2σ levels respectively. The flux variability on J1057+0012 and J1600−0037 is consistent with their core-jet classification. "Core-jet" sources are defined to show a one-sided jet, and the jet is often closely pointing to us (from a pole-on AGN). It is hard to estimate the real source size due to Doppler boosting, hence the "core-jet" sources might not be young radio sources even if they appear to be compact in some cases.

In addition, some sources are resolved out in our VLBI image by more than 10% of the total flux estimated from Table 1, probably due to diffuse emission associated with lobes and tail/jet emission. They are J0210+0419 (–14%), J0323+0534 (–38%), J0433−0229 (–18%), J1352+0232 (–15%), J1135+1107 (–31%), J2058+0540 (–12%), 2322−040 (–15%), and J1648+0242 is completely resolved out. The VLBI flux densities of the other nine sources at 1.6 GHz are consistent with the estimated total flux densities within an error of 10% the estimated of amplitude uncertainty of the EVN observations.

5. Summary and conclusion

1. We obtained total-intensity 1.6 GHz VLBI images of 17 GPS sources for the first time. The majority (80%) show a mini-double-lobe radio structure, indicating that they are CSOs or candidates and that their host AGNs could be edge-on to us. This result suggests that there is a high incidence of mini double-lobe sources and CSOs in the GPS source sample.
2. The sources J0323+0534, J1135−0021, J1352+0232, J2058+0540, 2121−014, and 2322−040 with measured redshift are double-lobed with sizes of <1 kpc and are classified as CSOs.
3. Three sources (J1057+0012, J1600−0037, and 1751+278) are classified as core-jet sources according to their morphologies and flux variability.
4. The 1.6 GHz images of the sources 0914+114, 1824+271, 2121−014, and 2322−040, for which we had observations at 2.3, 5.0, and 8.4 GHz, have provided information on their source structure and spectra at the lower frequency, permitting further spectral study in the future.

Acknowledgements. We thank the referee Alvaro Labiano and Nathan de Vries for comments. The European VLBI Network is a joint facility of European, Chinese, South African, and other radio astronomy institutes funded by their national research councils. This research has made use of the NASA/IPAC Extragalatic Database (NED), which is operated by the Jet Propulsion Laboratory, Caltech, under contract with NASA. This work was partly supported by the Natural Science Foundation of China (NSFC).

References

de Vries, W. H., Barthel, P. D., & O'Dea, C. P. 1997, A&A, 321, 105
de Vries, N., Snellen, I. A. G., Schilizzi, R. T., Lehnert, M. D., & Bremer, M. N. 2007, A&A, 464, 879
Dallacasa, D. 2004, in Proceedings of the 7th EVN Symposium, ed. R. Bachiller, F. Colomer, et al.
Fanti, C., Fanti, R., Dallacasa, D., et al. 1995, A&A, 302, 317
Gregory, P. C., & Condon, J. J. 1991, ApJS, 75, 1011
Griffith, M. R., Wright, A. E., Burke, B. F., & Ekers, R. D. 1995, ApJS, 97, 347
Labiano, A., Barthel, P. D., O'Dea, C. P., et al. 2007, A&A, 463, 97
Murgia, M. 2003, PASA, 20, 19
O'Dea, C. P. 1998, PASP, 110, 493
Orienti, M., Dallacasa, D., & Stanghellini, C. 2007, A&A, 461, 923
Owsianik, I., & Conway, J. E. 1998, A&A, 337, 69
Polatidis, A. G., & Conway, J. E. 2003, PASA, 20, 69
Snellen, I. A. G., Schilizzi, R. T., Miley, G. K., et al. 2000, MNRAS, 319, 445
Snellen, I. A. G., Lehnert, M. D., Bremer, M. N., & Schilizzi, R. T. 2002, MNRAS, 337, 981
Stanghellini, C., O'Dea, C. P., Dallacasa, D., et al. 1998, A&AS, 131, 303
Stanghellini, C., O'Dea, C. P., Dallacasa, D., et al. 2005, A&A, 443, 891
Tinti, S., Dallacasa, D., de Zotti, G., Celotti, A., & Stanghellini, C. 2005, A&A, 432, 31
Tschager, W., Schilizzi, R. T., Röttgering, H. J. A., Snellen, I. A. G., & Miley, G. K. 2000, A&A, 360, 887
Xiang, L., Stanghellini, C., Dallacasa, D., & Haiyan, Z. 2002, A&A, 385, 768
Xiang, L., Dallacasa, D., Cassaro, P., Jiang, D., & Reynolds, C. 2005, A&A, 434, 123
Xiang, L., Reynolds, C., Strom, R. G., & Dallacasa, D. 2006, A&A, 454, 729